ISSN 1070-3284, Russian Journal of Coordination Chemistry, 2020, Vol. 46, No. 7, pp. 466–476. © Pleiades Publishing, Ltd., 2020.
Russian Text © The Author(s), 2020, published in Koordinatsionnaya Khimiya, 2020, Vol. 46, No. 7, pp. 410–420.

Dedicated to I.L. Eremenko on the occasion of his 70th birthday

Mononuclear Antimony(V) Catecholate Complexes with Additional Pyridine Ligands

L. S. Okhlopkova[a], I. V. Smolyaninov[b], E. V. Baranov[a], and A. I. Poddel'skii[a, *]

[a] *Razuvaev Institute of Organometallic Chemistry, Russian Academy of Sciences, Nizhny Novgorod, 603600 Russia*
[b] *Southern Research Center, Russian Academy of Sciences, Rostov-on-Don, 344006 Russia*
**e-mail: aip@iomc.ras.ru*

Received December 27, 2019; revised January 30, 2020; accepted January 31, 2020

Abstract—A series of triarylantimony(V) complexes with *p*-dimethylaminopyridine and *p*-cyanopyridine of the general formulas [(Cat)$SbAr_3$(*p*-Me_2N–Py)] (complexes **I**–**IV**) and [(Cat)$SbAr_3$(*p*-CN–Py)] (complexes **V**–**VII**) has been synthesized. Their molecular structures and electrochemical properties have been studied. 3,6-Di-*tert*-butyl-*o*-benzoquinone, 4,5-piperazine-1,4-diyl-3,6-di-*tert*-butyl-*o*-benzoquinone, and 4,5-dichloro-3,6-di-*tert*-butyl-*o*-benzoquinone are used as redox-active ligands. The molecular structures of several complexes in the crystalline state are determined by X-ray diffraction analysis (CIF files CCDC nos. 1974173 (**I** · 0.5toluene), 1974174 (**II** · 2toluene), 1974175 (**V**), 1974176 (**VI** · hexane), and 1974177 (**VII**)). All complexes have a distorted octahedral structure, and an additional neutral pyridine ligand occupies one of the apical positions. Electrochemical transformations of the complexes are studied by cyclic voltammetry in a dichloromethane solution. The introduction of substituted pyridine into the molecule of the complex does not change the electrooxidation mechanism of the complexes. For all complexes with *p*-dimethylaminopyridine, both oxidation potentials are shifted to the cathodic region (0.13–0.21 V for the potential of the first oxidation process and to 0.3–0.4 V for the potential of the second oxidation process). A similar shift for the complex with *p*-cyanopyridine is less pronounced (0.05 V for the potential of the first oxidation process of complex **V** as compared to that of complex **I**).

Keywords: redox-active ligand, antimony(V), *o*-quinone, pyridine, X-ray diffraction analysis, cyclic voltammetry

DOI: 10.1134/S1070328420060081

INTRODUCTION

Some of the antimony(III/V) compounds are components of the metal-containing drugs, which have already been used for a long time in the clinical practice. The coordination and organometallic antimony compounds are characterized by a wide range of pharmacological activity provoking a constant interest in them [1–5]. The biological activity of the antimony(V) complexes was found to depend substantially on the type of ligands in the complexes. For example, the compounds with the sulfur-containing ligands are the most efficient drugs against some types of blood cancer, and the presence of halogens in the coordination sphere of antimony sometimes exerts a negative effect. Heterocyclic groups in many drugs are pharmacologically active. In the case of the antimony-containing organic compounds, the introduction of N-heterocyclic groups also demonstrates a positive dynamics compared to the oxygen-containing ligands [5]. Antimony(V) catecholates exhibit the antiradical and biological activity [6, 7]. The introduction of various additional neutral ligands into the antimony complexes can lead to both the shift of the oxidation potentials of the redox-active ligands to the cathodic or anodic range depending on the nature of the additional ligand and can completely change the mechanism of the redox transitions, which would result in a substantial change in the behavior of the corresponding complexes in diverse biochemical processes (for example, interception of free radicals, peroxide oxidation of lipids, and others).

In this work, we present the results of the studies of the molecular and electronic structures and specific features of the redox behavior of antimony(V) catecholates with *p*-dimethylaminopyridine and *p*-cyanopyridine of the general formulas [(Cat)$SbAr_3$(*p*-Me_2N–Py)] (**I**–**III**, Ar = Ph; **IV**, Ar = *p*-Tol) and [(Cat)$SbAr_3$(*p*-CN–Py)] (**V**, **VI**, Ar = Ph; **VII**, Ar = *p*-Tol).

EXPERIMENTAL

The complexes were synthesized and isolated and their properties were studied in evacuated ampules in the absence of oxygen. The organic solvents used in the work (THF, acetone, diethyl ether, toluene, pyridine, hexane, and pentane) were purified using standard procedures [8]. (3,6-Di-*tert*-butylcatecholato)triphenylantimony(V) [9], (3,6-di-*tert*-butylcatecholato)-tri-*p*-tolylantimony(V) [10], (4,5-(*N*,*N*′-diethylenediamino)-3,6-di-*tert*-butylcatecholato)triphenylantimony(V) [11], and (4,5-dichloro-3,6-di-*tert*-butylcatecholato)triphenylantimony(V) [12] were synthesized according to the described literature procedures.

^{1}H and ^{13}C{^{1}H} NMR spectra were recorded on Bruker AVANCE DPX-200 and Bruker Avance III spectrometers using tetramethylsilane as the internal standard and $CDCl_3$ as the solvent. IR spectra were recorded on FSM 1201 and Bruker VERTEX 70 FTIR spectrometers in Nujol.

Elemental analyses were carried out on a Euro EA 3000 C,H,N analyzer and using the method of pyrolytic decomposition in an oxygen flow.

Oxidation potentials were measured by cyclic voltammetry in a three-electrode cell using an IPC-pro potentiostat in an argon medium. A stationary glassy carbon (GC) electrode with a diameter of 2 mm was used as a working electrode, and a platinum wire (S = 18 mm^2) served as an auxiliary electrode. The reference electrode was Ag/AgCl/KCl_{sat} with a waterproof membrane. The potential sweep rate was 0.2 V/s.

Synthesis of the (3,6-di-*tert*-butylcatecholato)triphenyl-(*p*-dimethylaminopyridine)antimony(V) complex (3,6-DBCat)$SbPh_3$(*p*-Me_2N–Py) (I). A solution of (3,6-di-*tert*-butylcatecholato)triphenylantimony(V) (257 mg, 0.45 mmol) in toluene (20 mL) was gradually added to a solution of *p*-dimethylaminopyridine (54.9 mg, 0.45 mmol) in toluene (15 mL). The reaction occurred at room temperature for 30 min. After concentrating, the solution was kept at 0°C for 24 h. The formed finely crystalline precipitate was filtered off and dried in vacuo. Single crystals of **I** · 0.5toluene suitable for X-ray diffraction analysis (XRD) were obtained by recrystallization from a toluene–hexane (1 : 1) mixture. The yield was 0.31 g (92%).

For $C_{39}H_{45}N_2O_2Sb$ (**I**)

Anal. calcd., %	C, 67.35	H, 6.52	Sb, 17.51
Found, %	C, 67.21	H, 6.47	Sb, 17.37

IR (Nujol), ν, cm^{-1}: 1579 m, 1535 s, 1493 m, 1478 m, 1444 s, 1430 s, 1404 s, 1350 s, 1308 m, 1296 w, 1282 m, 1261 s, 1242 s, 1226 s, 1199 m, 1186 m, 1147 m, 1122 w, 1066 s, 1022 w, 1009 s, 976 s, 941 s, 926 w, 805 s, 789 m, 759 w, 736 s, 728 s, 694 s, 658 w, 645 m, 593 w, 543 w, 526 m, 465 m, 452 m. ^{1}H NMR ($CDCl_3$), δ, ppm: 1.41 (s, 18H, *t*-Bu), 2.95 (s, 6H, $(CH_3)_2N$), 6.27 (d, J = 7.0 Hz, 2H, Py), 6.55 (s, 2H, C_6H_2), 7.3–7.4 (m, 9 H, *o*,*p*-H, Ph), 7.7–7.8 (m, 6H, *m*-H, Ph), 7.94 (d, J = 7.0 Hz, 2H, Py). ^{13}C{^{1}H} NMR ($CDCl_3$), δ, ppm: 29.51 (CH_3, *t*-Bu), 34.09 (C, *t*-Bu), 39.09 ($(CH_3)_2N$), 105.76, 113.15, 128.20, 128.36 (*m*-C, $SbPh_3$), 129.01, 129.51 (*p*-C, $SbPh_3$), 131.88, 134.98 (*o*-C, $SbPh_3$), 143.14 (CO), 146.35 (CO), 146.74 (C–N), 154.82 (C_{ar}–N).

Synthesis of complexes II–VII was carried out using the method similar to that for complex **I**.

(4,5-(*N*,*N*′-Diethylenediamino-1,4-diyl)-3,6-di-*tert*-butylcatecholato)triphenyl(*p*-dimethylaminopyridine)antimony(V) (4,5-Pip-3,6-DBCat)$SbPh_3$(*p*-Me_2N–Py) (**II**) represents a yellow finely crystalline powder. The crystals of **II** · 2toluene suitable for XRD were isolated from a toluene–hexane (1 : 1) mixture. The yield was 88%.

For $C_{43}H_{51}N_4O_2Sb$ (**II**)

Anal. calcd., %	C, 66.41	H, 6.61	Sb, 15.66
Found, %	C, 66.15	H, 6.71	Sb, 15.48

IR (Nujol), ν, cm^{-1}: 1656 w, 1624 s, 1611 s, 1577 m, 1569 m, 1537 s, 1478 s, 1443 s, 1382 s, 1348 m, 1336 m, 1307 s, 1290 w, 1264 m, 1226 s, 1186 m, 1119 w, 1069 m, 1062 m, 1053 m, 1042 m, 1022 w, 1003 w, 995 s, 952 w, 934 m, 922 m, 898 w, 867 w, 855 s, 810 s, 771 m, 760 s, 740 s, 698 s, 656 m, 616 m, 592 w, 559 m, 531 s, 458 s. ^{1}H NMR ($CDCl_3$), δ, ppm: 1.59 (s, 18H, *t*-Bu), 2.55–2.69 (m, 4H, $N(CH_2CH_2)_2N$), 2.88–2.3.01 (m, 10H, $N(CH_2CH_2)_2N$ + $(CH_3)_2N$), 6.42 (d, J = 6.7 Hz, 2H, Py), 7.36–7.45 (m, 9H, *o*,*p*-H, Ph), 7.7–7.8 (m, 6H, *m*-H, Ph), 8.06 (d, J = 6.7 Hz, 2H, Py). ^{13}C{^{1}H} NMR ($CDCl_3$), δ, ppm: 30.06 (CH_3, *t*-Bu), 34.73 (C, *t*-Bu), 38.53, 49.51, 105.56, 124.64, 127.57, 128.03, 128.38, 129.28, 129.62, 134.05, 134.44, 137.21, 139.65, 140.07 (CO), 143.41 (CO), 146.79 (C–N), 154.15 (C_{ar}–N).

(4,5-Dichloro-3,6-di-*tert*-butylcatecholato)triphenyl(*p*-dimethylaminopyridine)antimony(V) (4,5-Cl_2-3,6-DBCat)$SbPh_3$(*p*-Me_2N–Py) (**III**) represents light yellow crystals isolated from a toluene–hexane (1 : 1) mixture. The yield was 91%.

For $C_{39}H_{43}N_2O_2Cl_2Sb$ (**III**)

Anal. calcd., %	C, 61.28	H, 5.67	Sb, 15.93
Found, %	C, 61.30	H, 5.61	Sb, 15.87

IR (Nujol), ν, cm^{-1}: 1646 s, 1618 s, 1569 s, 1494 m, 1432 m, 1395 s, 1317 m, 1246 m, 1222 s, 1204 m, 1135 s, 1066 m, 1030 w, 1023 w, 1004 m, 997 m, 978 m, 840 s, 774 w, 752 m, 732 s, 694 s, 669 w, 656 w, 615 w, 561 w, 544 w, 480 w, 461 m. ^{1}H NMR ($CDCl_3$), δ, ppm: 1.60 (s, 18H, *t*-Bu), 2.94 (s, $(CH_3)_2N$), 6.23 (d, J = 7.1 Hz, 2H, Py), 7.32–7.40 (m, 9H, *o*,*p*-H, Ph), 7.62–7.71 (m, 6H, *m*-H, Ph), 7.78 (d, J = 7.1 Hz, 2H, Py).

$^{13}C\{^1H\}$ NMR ($CDCl_3$), δ, ppm: 29.63 (CH_3, *t*-Bu), 32.34 (C, *t*-Bu), 38.48 and 39.03 ($(CH_3)_2N$), 105.6 (C_{ar}–Cl), 122.11, 128.25 (*m*-C, $SbPh_3$), 128.85 and 128.99 (C_{ar}–Py), 129.34 (*p*-C, $SbPh_3$), 134.82 (*o*-C, $SbPh_3$), 136.20, 147.13 (CO), 154.69 (C_{ar}–$N(CH_3)_2$).

(3,6-Di-*tert*-butylcatecholato)tri-*p*-tolyl-(*p*-dimethylaminopyridine)antimony(V) (3,6-DBCat)Sb(*p*-Tol)$_3$(*p*-Me_2N–Py) (**IV**) represents a yellow finely crystalline powder isolated from a toluene–hexane (1 : 1) mixture. The yield was 91%.

For $C_{42}H_{51}N_2O_2Sb$ (**IV**)

Anal. calcd., %	C, 68.39	H, 6.92	Sb, 16.55
Found, %	C, 68.28	H, 6.71	Sb, 16.28

IR (Nujol), ν, cm^{-1}: 1622 s, 1614 s, 1536 s, 1403 s, 1350 s, 1307 m, 1294 m, 1282 m, 1261 m, 1243 m, 1228 s, 1203 s, 1187 s, 1146 m, 1118 m, 1062 s, 1004 s, 976 s, 940 s, 923 m, 809 s, 794 s, 758 m, 721 m, 707 w, 689 m, 647 m, 594 w, 576 m, 544 w, 526 m, 485 s, 461 w. ^1H NMR ($CDCl_3$), δ, ppm: 1.41 (s, 18H, *t*-Bu), 2.36 (s, 3CH_3, Sb(*p*-Tol)), 2.98(s, 6H, $(CH_3)_2N$), 6.37 (d, *J* = 6.1 Hz, 2H, Py), 6.55 (s, 2H, C_6H_2), 7.19 (d, *J* = 7.7 Hz, 6H, Sb(*p*-Tol)), 7.64 (d, *J* = 7.9 Hz, 6H, Sb(*p*-Tol)), 8.02 (d, *J* = 6.1 Hz, 2H, Py). $^{13}C\{^1H\}$ NMR ($CDCl_3$), δ, ppm: 21.42 (CH_3, Tol), 29.55 (CH_3, *t*-Bu), 34.09 (C, *t*-Bu), 39.14 ($(CH_3)_2N$), 106.03, 113.34, 125.28, 128.21, 129.02, 129.31 (*m*-C, Sb(*p*-Tol)$_3$), 131.84, 134.94 (*o*-C, Sb(*p*-Tol)$_3$), 139.92, 146.10, 146.92.

(3,6-Di-*tert*-butylcatecholato)triphenyl(*p*-cyanopyridine)antimony(V) (3,6-DBCat)$SbPh_3$(*p*-CN–Py) (**V**) represents a yellow crystalline product isolated from a toluene–hexane (1 : 1) mixture. The yield was 81%. The crystals of complex **V** suitable for XRD were obtained by prolonged recrystallization from a toluene–hexane (1 : 1) mixture.

For $C_{38}H_{39}N_2O_2Sb$ (**V**)

Anal. calcd., %	C, 67.37	H, 5.80	Sb, 17.97
Found, %	C, 67.40	H, 5.81	Sb, 17.87

IR (Nujol), ν, cm^{-1}: 1645 w, 1602 m, 1576 w, 1550 w, 1433 s, 1403 s, 1354 m, 1306 w, 1282 m, 1264 m, 1240 s, 1183 w, 1143 m, 1089 w, 1067 m, 1024 m, 1002 m, 996 m, 977 s, 941 m, 926 m, 871 w, 858 w, 829 m, 817 m, 808 m, 794 m, 769 w, 735 s, 694 s, 661 w, 647 m, 600 w, 558 s, 515 w, 456 s. ^1H NMR ($CDCl_3$), δ, ppm: 1.47 (s, 18H, *t*-Bu), 6.66 (s, 2H, C_6H_2), 7.4–7.55 (m, 11H, *o*-,*p*-H, 3Ph + 2H, Py), 7.77–7.89 (m, 6H, *m*-H, 3Ph), 8.78 (d, *J* = 5.9 Hz, 2H, Py). $^{13}C\{^1H\}$ NMR ($CDCl_3$), δ, ppm: 29.53 (CH_3, *t*-Bu), 34.10 (C, *t*-Bu), 114.21, 116.29, 120.49, 125.18, 129.02 (*m*-C, $SbPh_3$), 130.88 (*p*-C, $SbPh_3$), 132.07, 134.94 (*o*-C, $SbPh_3$), 136.18 (*i*-C, $SbPh_3$), 138.50, 145.26 (CO), 150.58 (C≡N).

(4,5-Dichloro-3,6-di-*tert*-butylcatecholato)triphenyl(*p*-cyanopyridine)antimony(V) (4,5-Cl_2-3,6-DBCat)$SbPh_3$(*p*-CN–Py) (**VI**) represents light yellow crystals isolated from toluene. The yield was 78%. The crystals of complex **VI** · hexane suitable for XRD were isolated from a toluene–hexane (1 : 1) mixture.

For $C_{38}H_3N_2O_2Cl_2Sb$ (**VI**)

Anal. calcd., %	C, 61.15	H, 5.00	Sb, 16.31
Found, %	C, 61.10	H, 5.02	Sb, 16.37

IR (Nujol), ν, cm^{-1}: 1656 w, 1603 m, 1592 m, 1579 w, 1551 m, 1494 m, 1479 s, 1434 s, 1410 s, 1395 s, 1331 w, 1307 w, 1247 s, 1210 s, 1158 w, 1065 s, 1031 m, 1023 m, 997 s, 926 w, 842 s, 776 s, 731 s, 695 s, 671 w, 662 w, 633 w, 590 w, 562 s, 500 s, 455 s. ^1H NMR ($CDCl_3$), δ, ppm: 1.63 (s, 18H, *t*-Bu), 7.4–7.56 (m, 11H, *o*, *p*-H, 3Ph + 2H, Py), 7.68–7.77 (m, 6H, *m*-H, 3Ph), 8.76 (d, *J* = 5.1 Hz, 2H, Py). $^{13}C\{^1H\}$ NMR ($CDCl_3$), δ, ppm: 32.20 (CH_3, *t*-Bu), 38.47 (C, *t*-Bu), 120.51, 123.62, 125.20, 129.22 (*m*-C, $SbPh_3$), 129.71, 131.19 (*p*-C, $SbPh_3$), 134.70 (*o*-C, $SbPh_3$), 137.57, 145.56 (CO), 150.61.

(3,6-Di-*tert*-butylcatecholato)tri-*p*-tolyl(*p*-cyanopyridine)antimony(V) (3,6-DBCat)Sb(*p*-Tol)$_3$(*p*-CN–Py) (**VII**) represents a yellow crystalline product isolated from a toluene–hexane (1 : 1) mixture. The yield was 80%. The crystals suitable for XRD were obtained by the prolonged crystallization from this mixture.

For $C_{41}H_{45}N_2O_2Sb$ (**VII**)

Anal. calcd., %	C, 68.43	H, 6.26	Sb, 16.97
Found, %	C, 68.40	H, 6.28	Sb, 16.87

IR (Nujol), ν, cm^{-1}: 1632 w, 1600 m, 1550 m, 1490 s, 1407 s, 1350 m, 1306 w, 1280 m, 1260 s, 1240 s, 1221 m, 1208 m, 1186 s, 1142 m, 1115 w, 1070 s, 1060 m, 1026 w, 1018 w, 1004 m, 976 s, 939 s, 925 w, 854 w, 824 s, 810 s, 796 s, 766 w, 731 w, 693 s, 646 s. ^1H NMR ($CDCl_3$), δ, ppm: 1.44 (s, 18H, *t*-Bu), 2.39 (s, 9H, CH_3, *p*-Tol), 6.61 (s, 2H, C_6H_2), 7.26 (d, *J* = 7.6 Hz, 6H, *p*-Tol), 7.53 (d, *J* = 5.1 Hz, 2H, Py), 7.68 (d, *J* = 7.6 Hz, 6H, *p*-Tol), 8.81 (d, *J* = 5.1 Hz, 2H, Py). $^{13}C\{^1H\}$ NMR ($CDCl_3$), δ, ppm: 21.46 (CH_3, *p*-Tol), 29.59 (CH_3, *t*-Bu), 34.12 (C, *t*-Bu), 114.06, 125.20, 129.76 (*m*-C, Sb(*p*-Tol)$_3$), 131.98, 134.96 (*o*-C, Sb(*p*-Tol)$_3$), 141.10, 145.43, 150.76.

XRD analyses of the single crystals of complexes **I** · 0.5toluene, **II** · 2toluene, **V**, **VI** · hexane, and **VII** were carried out on Bruker SMART APEX (for **I** · 0.5toluene), Bruker D8 Quest (for **II** · 2toluene), and Agilent Xcalibur E (for **V**, **VI** · hexane, and **VII**) automated diffractometers (ω and φ scan modes, MoK_α radiation, λ = 0.71073 Å). Experimental sets of intensities were integrated using the SAINT [13] for **I** · 0.5toluene and **II** · 2toluene and CrysAlisPro [14] programs for **V**, **VI** ·

Table 1. Crystallographic data and structure refinement parameters for compounds **I**, **II**, and **V**–**VII**

Parameter	Value				
	I · 0.5toluene	**II** · 2toluene	**V**	**VI** · hexane	**VII**
Empirical formula	$C_{42.5}H_{49}O_2N_2Sb$	$C_{57}H_{67}O_2N_4Sb$	$C_{38}H_{39}O_2N_2Sb$	$C_{44}H_{51}N_2O_2Cl_2Sb$	$C_{41}H_{45}N_2O_2Sb$
FW	741.58	961.89	677.46	832.52	719.54
T, K	100(2)	100(2)	100(2)	110(2)	100(2)
Crystal system	Triclinic	Triclinic	Orthorhombic	Triclinic	Orthorhombic
Space group	$P\bar{1}$	$P\bar{1}$	*Pbca*	$P\bar{1}$	*Pbca*
a, Å	9.8596(2)	11.8832(4)	17.1642(2)	12.7842(2)	19.9189(3)
b, Å	12.7594(3)	14.7336(5)	20.0849(2)	17.4809(2)	18.0331(3)
c, Å	15.4334(4)	15.2983(5)	38.6509(3)	18.9108(2)	20.2776(3)
α, deg	72.988(1)	96.899(1)	90	104.599(1)	90
β, deg	83.776(1)	108.963(1)	90	97.203(1)	90
γ, deg	80.734(1)	101.937(1)	90	93.644(1)	90
V, Å	1828.51(7)	2426.99(14)	13 324.6(2)	4037.47(9)	7283.7(2)
Z	2	2	16	4	8
ρ_{calc}, g cm^{-3}	1.347	1.316	1.351	1.370	1.312
μ, mm^{-1}	0.792	0.615	0.863	0.854	0.793
F(000)	770	1008	5568	1720	2976
Range of measuring θ, deg	2.10–28.00	2.23–30.20	2.83–26.02	2.92–26.02	3.02–28.00
Number of reflections	18424	36034	188914	61677	122083
Number of independent reflections	8704	14374	13109	15892	8775
R_{int}	0.0111	0.0268	0.0511	0.0319	0.0583
Goodness-of-fit (F^2)	1.060	1.057	1.049	1.090	1.069
R_1/wR_2 ($I > 2\sigma(I)$)	0.0195/ 0.0485	0.0264/0.0564	0.0374/0.0793	0.0413/ 0.1028	0.0315/0.0768
R_1/wR_2 (for all parameters)	0.0202/0.0489	0.0325/0.0582	0.0429/0.0818	0.0463/0.1050	0.0453/0.0821
$\Delta\rho_{max}/\Delta\rho_{min}$, e Å^{-3}	0.905/–0.279	0.455/–0.452	4.000/–1.007	1.483/–0.825	2.826/–0.901

hexane, and **VII**. All structures were solved by the "dual-space" method using the SHELXT program [15]. Non-hydrogen atoms were refined by full-matrix least squares for F^2_{hkl} in the anisotropic approximation using the SHELXTL program package [16]. Hydrogen atoms were placed in the geometrically calculated positions and refined isotropically. An absorption correction was applied using the SADABS [17] for **I** · 0.5toluene and **II** · 2toluene and SCALE3 ABSPACK [18] programs for **V**, **VI** · hexane, and **VII**. The crystals of **I** · 0.5toluene, **II** · 2toluene, and **VI** · hexane contain toluene and *n*-hexane solvate molecules, respectively, in the 0.5 : 1, 2 : 1, and 1 : 1 ratios to the antimony complex. The solvate molecules in **I** · 0.5toluene and **VI** · hexane are disordered over two positions. One of the phenyl substituents in one of two independent molecules of antimony complex **V** is disordered over two positions. Selected crystallographic data and XRD experimental parameters are presented in Table 1.

The structural data for the crystals of new complexes were deposited with the Cambridge Crystallographic Data Centre (CIF files CCDC nos. 1974173 (**I** · 0.5toluene), 1974174 (**II** · 2toluene), 1974175 (**V**), 1974176 (**VI** · hexane), and 1974177 (**VII**); ccdc.cam.ac.uk/getstructures).

RESULTS AND DISCUSSION

As shown above, antimony in the highest oxidation state tends to the hexacoordinated environment. This occurs due to either intermolecular interactions, or the coordination of solvent molecules. However, this process can purposefully be controlled by the introduction of an additional donor ligand into the reactions. The interaction of (3,6-di-*tert*-butylcatecholato)triphenyl- or tri-*p*-tolylantimony(V), (4,5-(*N*,*N*'-diethylenediamino)-3,6-di-*tert*-butylcatecholato)triphenylantimony(V), and (4,5-dichloro-3,6-di-*tert*-butylcatecholato)triphenylantimony(V) with *p*-dimethylaminopyridine in toluene results in the coordination of the pyridine group of the neutral ligand to the antimony atom to form the corresponding products **I**–**IV** (Scheme 1).

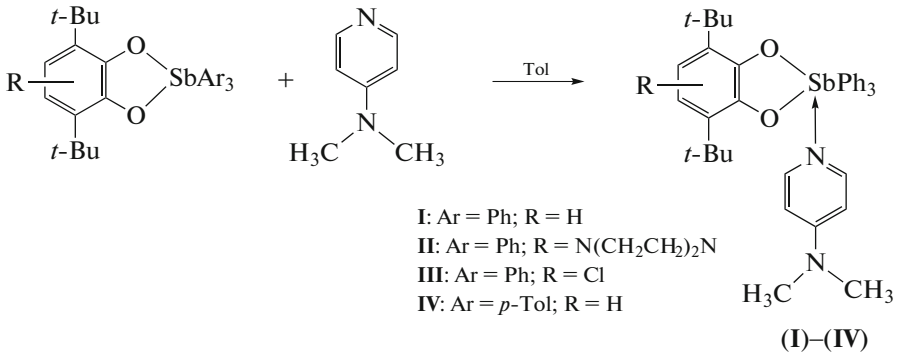

Scheme 1.

Compounds **I**–**IV** were isolated in the individual state by crystallization directly from the reaction mixtures almost in quantitative yields and represent yellow finely crystalline substances highly soluble in polar solvents (their solubility in nonpolar solvents is lower). The obtained complexes are diamagnetic and exhibit well resolved solution NMR spectra, which are consistent with the proposed formulas. The IR spectra contain the intense absorption bands in a range of 1580–1380 cm^{-1} characteristic of aromatic C=C and C = N bonds [19] and the bands in a range of 1200–1000 cm^{-1} characteristic of ordinary C–O and C–N bonds. The IR spectra also contain sets of bands corresponding to vibrations of other functional groups in the composition of the complexes: stretching vibrations of the Sb–C_{Ph} bonds in a range of 510–450 cm^{-1} and of the Sb–O bonds at 620–650 cm^{-1} and bending vibrations of Sb–Ph_3 at 940–690 cm^{-1}.

All complexes **I**–**IV** are stable under usual conditions and resistant to air oxygen (in the solid state). The molecular structures of complexes **I** and **II** in the crystalline state were determined by the XRD method (Figs. 1 and 2).

In the molecules of complexes **I** and **II**, the catecholate fragment and two phenyl groups lie in the base of the distorted octahedron, and the third phenyl group and N-donor substituent occupy the apical positions. The antimony atom shifts from the plane of the octahedron base by 0.202 (**I**) and 0.251 Å (**II**), deviating from the neutral donor ligand. The angles between the equatorial and axial substituents lie in the range 79.58(4)°–104.45(5)°, and the angles between the axial substituents are 171.89(4)° and 172.25(4)°, respectively. The sum of the OSbO, OSbPh, and PhSbPh angles in the equatorial plane of complex **I** is 357.93°, and that for complex **II** is 356.69°. The five-membered SbOOCC cycle is nearly planar in both complexes, and the inflection angle along the O...O line toward the catecholate ligand plane is 3.98° in complex **I** and 1.05° in complex **II**. In both compounds, the C(1)–O(1), C(2)–O(2) bond lengths are characteristic of the catecholate form of the *o*-quinone ligand (1.33–1.39 Å [20–23]) and are equal to 1.360(2), 1.357(1) and 1.355(2), 1.354(2) Å, respectively. The Sb–O distances (Sb(1)–O(1) and Sb(1)–O(2)) in complex **I** are 2.042(1) and 2.045(1) Å, and

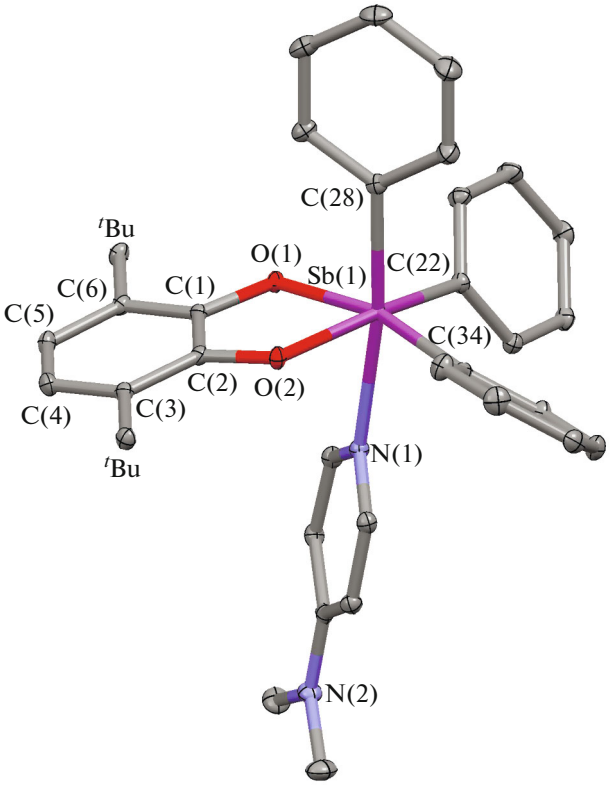

Fig. 1. Molecular structure of complex **I** in the crystalline state. Hydrogen atoms and the methyl groups of the *tert*-butyl substituents are omitted (thermal ellipsoids of 50% probability). Selected bond lengths and angles in complex **I**: Sb(1)–O(1) 2.042(1), Sb(1)–O(2) 2.045(1), Sb(1)–C(22) 2.160(1), Sb(1)–C(28) 2.156(1), Sb(1)–C(34) 2.147(1), Sb(1)–N(1) 2.343(1), O(1)–C(1) 1.360(2), O(2)–C(2) 1.357(1) Å and O(1)Sb(1)O(2) 79.51(3)°, O(1)Sb(1)C(34) 164.59(4)°, O(2)Sb(1)C(34) 87.07(4)°, O(1)Sb(1)C(28) 91.12(4)°, O(2)Sb(1)C(28) 94.78(4)°, C(34)Sb(1)C(28) 97.57(5)°, O(1)Sb(1)C(22) 86.90(4)°, (2)Sb(1)C(22) 161.86(4)°, C(34)Sb(1)C(22) 104.45(5)°, C(28)Sb(1)-C(22) 97.47(5)°, O(1)Sb(1)N(1) 82.28(4)°, O(2)Sb(1)-N(1) 80.07(4)°, C(34)Sb(1)N(1) 88.02(4)°, C(28)Sb(1)-N(1) 172.25(4)° C(22)Sb(1)N(1) 86.28(4)°, C(1)O(1)-Sb(1) 113.72(7)°, C(2)O(2)Sb(1) 113.59(7)°.

those in complex **II** are 2.033(1) and 2.034(1) Å. The Sb–C distances range from 2.146(1) to 2.160(1) Å. The Sb–N bond lengths (2.343(1) and 2.414(1) Å) corresponding to the antimony–nitrogen donor–acceptor bond are typical of similar compounds [24].

The electrochemical transformations of complexes **I**–**IV** were studied by cyclic voltammetry (CV) in a dichloromethane solution. The values obtained for the electrode potentials of the complexes are nearly independent of the material of the electrode. The corresponding electrochemical characteristics are presented in Table 2.

The earlier studied catecholate derivatives are characterized by two redox transitions: catecholate–*o*-benzosemiquinone and *o*-benzosemiquinone–*o*-benzoquinone. The initial triphenylantimony(V) catecholates are oxidized via two consecutive one-electron oxidation steps, the first of which is reversible, while the second step is irreversible [25, 26]. The introduction of pyridine with the donor dimethylamine group into the para position of the complex does not change the electrooxidation mechanism of the complexes (Scheme 2).

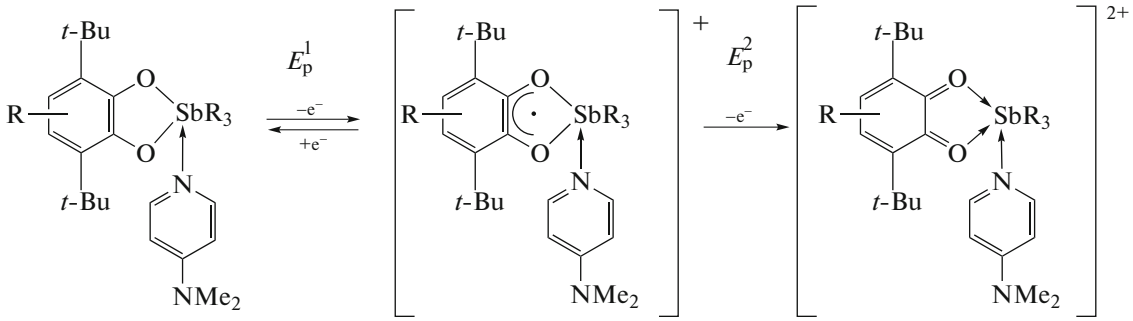

Scheme 2.

For all complexes, both oxidation potentials are substantially shifted to the cathodic range. No additional redox transitions are observed when the potential sweep range is extended to 1.8 V. Complexes **I** and

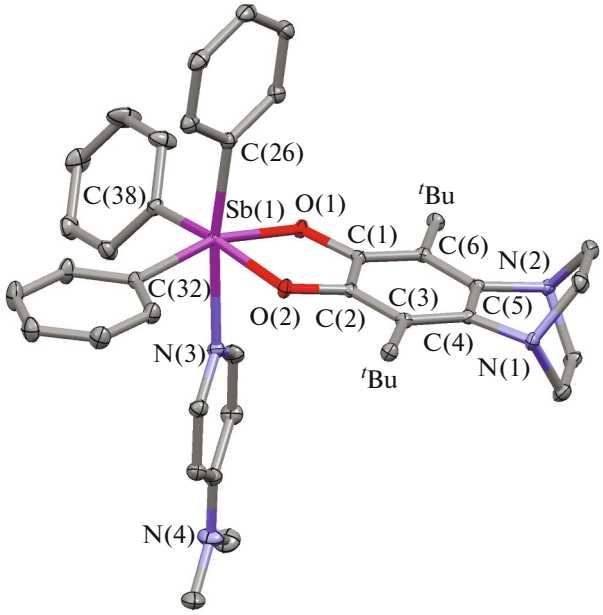

Fig. 2. Molecular structure of complex **II** in the crystalline state. Hydrogen atoms and the methyl groups of the *tert*-butyl substituents are omitted (thermal ellipsoids of 50% probability). Selected bond lengths and angles in complex **II**: (1)–O(1) 2.033(1), Sb(1)–O(2) 2.034(1), Sb(1)–N(3) 2.414(1), Sb(1)–C(26) 2.146(1), Sb(1)–C(32) 2.146(1), Sb(1)–C(38) 2.151(1), O(1)–C(1) 1.355(2), O(2)–C(2) 1.354(2) Å and O(1)Sb(1)O(2) 78.95(4)°, O(1)Sb(1)C(32) 162.65(4)°, O(2)Sb(1)C(32) 87.75(4)°, O(1)Sb(1)C(26) 93.35(4)°, O(2)Sb(1)C(26) 94.68(4)°, C(32)Sb(1)C(26) 98.85(5)°, O(1)Sb(1)C(38) 88.30(4)°, O(2)Sb(1)C(38) 161.42(4)°, C(32)Sb(1)C(38) 101.69(5)°, C(26)Sb(1)C(38) 99.56(5)°, O(1)Sb(1)N(3) 79.58(4)°, O(2)Sb(1)N(3) 80.15(4)°, C(32)Sb(1)N(3) 87.25(4)°, C(26)Sb(1)N(3) 171.89(4)°, C(38)Sb(1)N(3) 84.31(4)°, C(1)O(1)Sb(1) 115.17(8)°, C(2)O(2)Sb(1) 114.89(8)°.

Table 2. Electrochemical potentials of complexes **I**–**V** according to the CV data*

Compound	Parameters**			
	E^1_{pa}, V	N	E^2_{pa}, V	E^3_{pa}, V
(3,6-DBCat)$SbPh_3$ [13]	0.96	1	1.40	
(4,5-Pip-3,6-DBCat)$SbPh_3$ [13]	0.76	1	1.23	1.48
(4,5-Cl_2-3,6-DBCat)$SbPh_3$ [13]	1.03	1	1.33	
(3,6-DBCat)$SbPh_3$(*p*-Me_2N–Py) (**I**)	0.75	1	0.96	
(4,5-Pip-3,6-DBCat)$SbPh_3$(*p*-Me_2N–Py) (**II**)	0.63	1	0.81	1.49
(4,5-Cl_2-3,6-DBCat)$SbPh_3$(*p*-Me_2N–Py) (**III**)	0.85	1	1.02	
(3,6-DBCat)Sb(p-Tol)$_3$(*p*-Me_2N–Py) (**IV**)	0.74	1	0.93	
(3,6-DBCat)$SbPh_3$(*p*-CN–Py) (**V**)	0.91	>1	1.40	

* (GC electrode, CH_2Cl_2, $V = 0.2$ V/s, 0.1 M NBu_4ClO_4, $c = 3 \times 10^{-3}$ mol/L, Ar, vs. Ag/AgCl/KCl_{sat}).

** E^1_{pa} is the peak potential of the first anodic process, N is the number of electrons of the first anodic step vs. ferrocene as the standard, E^2_{pa} is the peak potential of the second oxidation process, and E^3_{pa} is the peak potential of the third oxidation peak.

IV are oxidized at almost the same values; i.e., the replacement of the phenyl groups by *p*-tolyl groups exerts no substantial effect on the redox properties. The first redox transition for complex **III** is quasi-reversible, which is related to the presence of the electron-acceptor chlorine atoms in the catecholate ligand stabilizing the formed monocation during the first oxidation wave. However, the peak at –0.34 V on the reverse CV branch indicates a low stability of the generated monocation and the fast chemical reaction in the solution leading to a product, whose reduction peak is detected on the CV curve. The voltammograms of complex **II** have the following specific features: the second oxidation peak of the initial complex at 1.23 V nearly disappears and a new anodic peak is detected at 0.81 V. The third anodic peak remains almost unchanged in both the initial complex and the complex containing the additional ligand. Complex **II** also remains sensitive to air oxygen, and the oxidation peak of spiroendoperoxide appears with time on the CV curve at 1.32 V.

Pyridines with the donor substituents were used in the above described syntheses. Pyridine bearing the acceptor group in position 4 (*p*-cyanopyridine) was chosen as the subsequent N-ligand to consider the problem in more detail. (3,6-Di-*tert*-butylcatecholato)triphenyl(*p*-cyanopyridine)antimony(V) (**V**), (4,5-dichloro-3,6-di-*tert*-butylcatecholato)triphenyl(*p*-cyanopyridine)antimony(V) (**VI**), and (3,6-di-*tert*-butylcatecholato)tri-*p*-tolyl(*p*-cyanopyridine)antimony(V) (**VII**) were synthesized (Scheme 3).

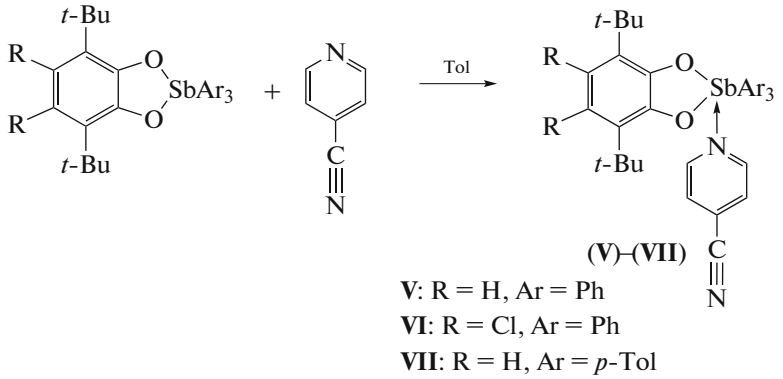

V: R = H, Ar = Ph
VI: R = Cl, Ar = Ph
VII: R = H, Ar = *p*-Tol

Scheme 3.

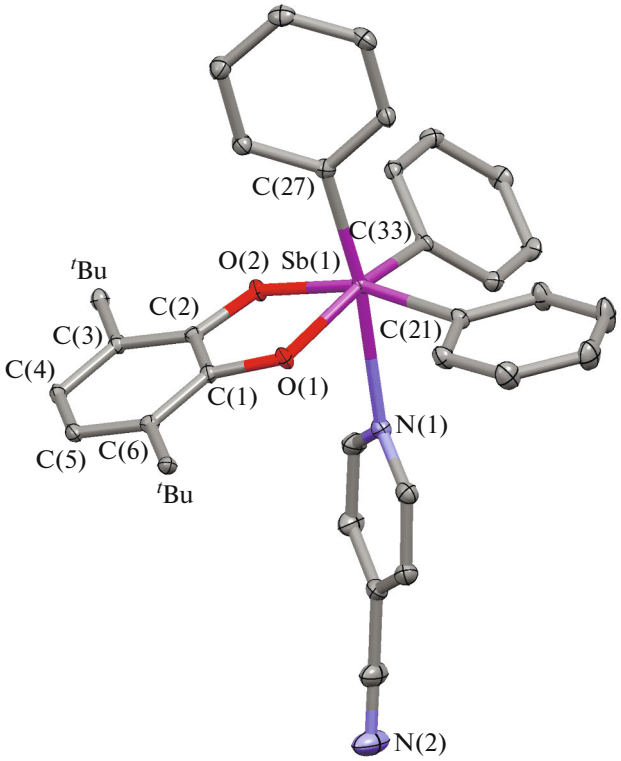

Fig. 3. Molecular structure of complex **V** in the crystalline state. Hydrogen atoms and the methyl groups of the *tert*-butyl substituents are omitted (thermal ellipsoids of 50% probability). Selected bond lengths and angles in complex**V**: Sb(1)–O(1) 2.028(2), Sb(1)–O(2) 2.045(2), Sb(1)– C(21) 2.144(3), Sb(1)–C(27) 2.149(3), Sb(1)–C(33) 2.104(3), Sb(1)–N(1) 2.600(3) Å and O(1)Sb(1)O(2) 79.67(8)°, O(1)Sb(1)C(33) 94.12(19)°, O(2)Sb(1)C(33) 93.56(14)°, O(1)Sb(1)C(21) 158.26(10)°, O(2)Sb(1)C(21) 86.33(9)°, C(33)Sb(1)C(21) 103.34(19)°, O(1)Sb(1)C(27) 87.71(10)°, O(2)Sb(1)C(27) 161.70(10)°, C(33)Sb(1)C(27) 100.56(15)°, C(21)Sb(1)C(27) 101.49(11)°.

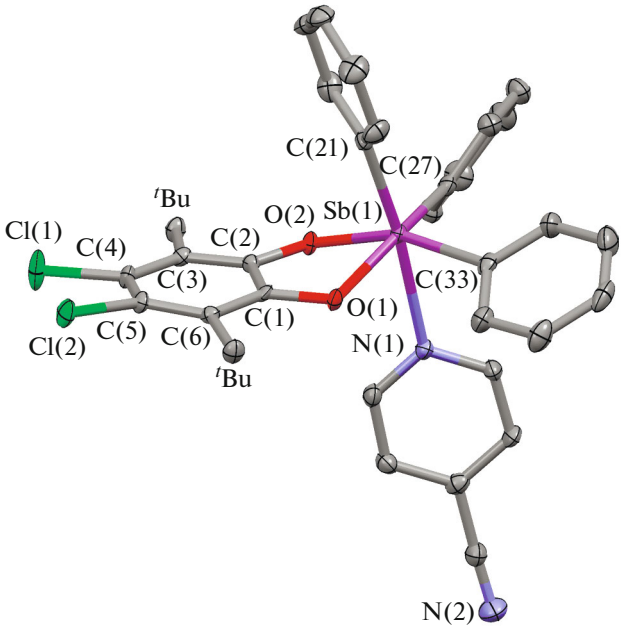

Fig. 4. Molecular structure of complex **VI** in the crystalline state. Hydrogen atoms and the methyl groups of the *tert*-butyl substituents are omitted (thermal ellipsoids of 50% probability). Selected bond lengths and angles in complex **VI**: Sb(1)–O(1) 2.036(3), Sb(1)–O(2) 2.039(3), Sb(1)–C(21) 2.141(4), Sb(1)–C(27) 2.150(4), Sb(1)–C(33) 2.154(4), Sb(1)–N(1) 2.470(3), O(1)–C(1) 1.359(4), O(2)–C(2) 1.363(4) Å and O(1)Sb(1)O(2) 77.75(10)°, O(1)Sb(1)C(21) 93.56(13)°, O(2)Sb(1)C(21) 96.23(13)°, O(1)Sb(1)C(27) 159.58(13)°, O(2)Sb(1)C(27) 85.27(13)°, C(21)Sb(1)C(27) 99.55(15)°, O(1)Sb(1)C(33) 88.64(13)°, O(2)Sb(1)C(33) 159.91(13)°, C(21)Sb(1)-C(33) 99.34(14)°, C(27)Sb(1)C(33) 104.46(15)°, O(1)-Sb(1)N(1) 80.14(11)°, O(2)Sb(1)N(1) 80.09(11)°.

Complexes **V**–**VII** were isolated in the individual state, and their structures were confirmed by IR and NMR spectroscopy, elemental analysis, and XRD. The molecular structures of complexes **V**–**VII** are shown in Figs. 3, 4, and 5, respectively.

According to the XRD data, the asymmetric part of the crystalline cell of compounds **V** and **VI** contains two independent molecules of the antimony complexes with similar geometric parameters. All complexes are characterized by a distorted octahedral configuration. The geometric characteristics of the redox-active ligand correspond to its catecholate form, and the six-membered carbon rings are aromatic [27–33]. The hexacoordinated complexes (**V** and **VI**) in crystals are packed in pairs in such a way that intermolecular interactions are observed between the nitrogen and carbon atoms of the adjacent cyano groups in (3,6-DBCat)$SbPh_3$(*p*-CN–Py) and between the chlorine atom and methyl carbon of the *tert*-butyl group in (4,5-Cl_2-3,6-DBCat)$SbPh_3$(*p*-CN–Py) (Fig. 6). The distance between the N and C atoms is 3.219 Å (**V**), and that between the Cl and C atoms is 3.321 Å (**VI**), which is significantly more than the sum of covalent radii of the considered atoms but is less than the sum of their van der Waals radii [34].

The XRD study of the crystals of complex **VII** (Fig. 5) shows that its geometric characteristics are similar to those of the above described complexes **V** and **VI**. Only an increase in the dihedral angle between the Sb(1)O(1)O(2) and Sb(1)C(15)C(29) planes to 26.45° over 23.25° (**V**) and 21.88° (**VI**) and short interactions between the nitrogen atom of the nitrile group and the hydrogen atoms of the *tert*-butyl groups with the N...H distance equal to 2.657–2.691 Å are observed.

The electrochemical oxidation potential of complex **V** in the first step (Table 2, Fig. 7) is shifted by 50 mV to the cathodic range compared to the first oxidation potential of the initial catecholate (3,6-

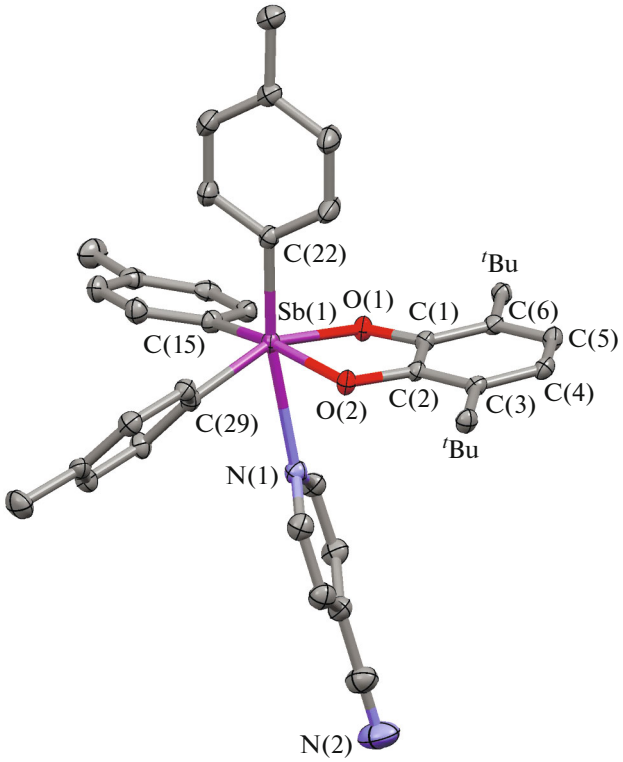

Fig. 5. Molecular structure of complex **VII** in the crystalline state. Hydrogen atoms and the methyl groups of the *tert*-butyl substituents are omitted (thermal ellipsoids of 50% probability). Selected bond lengths and angles in complex **VII**: Sb(1)–O(1) 2.024(1), Sb(1)–O(2) 2.050(1), Sb(1)–C(15) 2.150(2), Sb(1)–C(22) 2.133(2), Sb(1)–C(29) 2.129(2), Sb(1)–N(1) 2.603(2), O(1)–C(1) 1.364(2), O(2)–C(2) 1.360(2) Å and O(1)Sb(1)O(2) 79.41(6)°, O(1)Sb(1)C(29) 156.68(7)°, O(2)Sb(1)C(29) 87.77(7)°, O(1)Sb(1)C(22) 97.28(7)°, O(2)Sb(1)C(22) 94.04(7)°, C(29)Sb(1)C(22) 103.04(8)°, O(1)Sb(1)C(15) 87.30(7)°, O(2)Sb(1)C(15) 161.14(7)°, C(29)Sb(1)C(15) 99.84(8)°, C(22)Sb(1)C(15) 100.92(8)°, O(1)Sb(1)N(1) 77.24(6)°, O(2)Sb(1)(1) 76.58(6)°.

DBCat)$SbPh_3$ (Table 2). Note that the ratio of the first and second peaks changes. The second anodic peak is less pronounced, whereas the first anodic peak exceeds the one-electron level. The first electrode process is quasi-reversible (E^1_{pa} = 0.91 V). However, unlike the initial complex, the stability of the generated intermediate decreases, since the current ratio decreased to 0.45 compared to that for the initial compound.

Thus, a series of the hexacoordinated triarylantimony catecholate complexes based on various *o*-benzoquinones with *p*-dimethylamino- and *p*-cyanopyridine was synthesized. Their molecular structures and electrochemical properties were studied. The presence of the pyridine ligand was shown to exert no effect on the mechanism of the electrochemical oxidation of the complexes but to affect the first and second oxidation potentials shifting them to the cathodic range. The influence of *p*-dimethylaminopyridine is more pronounced, the shift of the first oxidation potential is 0.1–0.2 V, and the second oxidation potential is shifted to 0.4 V, whereas the shift of the first oxidation potential for *p*-cyanopyridine is 0.05 V only.

ACKNOWLEDGMENTS

The study was carried out using the equipment of "Analytical Center of the IOMC RAS" (Zentr Kolektivnogo Polzovaniya) in G.A. Razuvaev Institute of Organometallic Chemistry RAS with the financial support of the Federal objective program "Research and development in priority directions of advancement of science and technology complex of Russia for 2014-2020" (Unique project identifier is RFMEFI62120X0040).

FUNDING

This work was performed in the accordance with the state assignment of the Razuvaev Institute of Organometallic Chemistry (Russian Academy of Sciences).

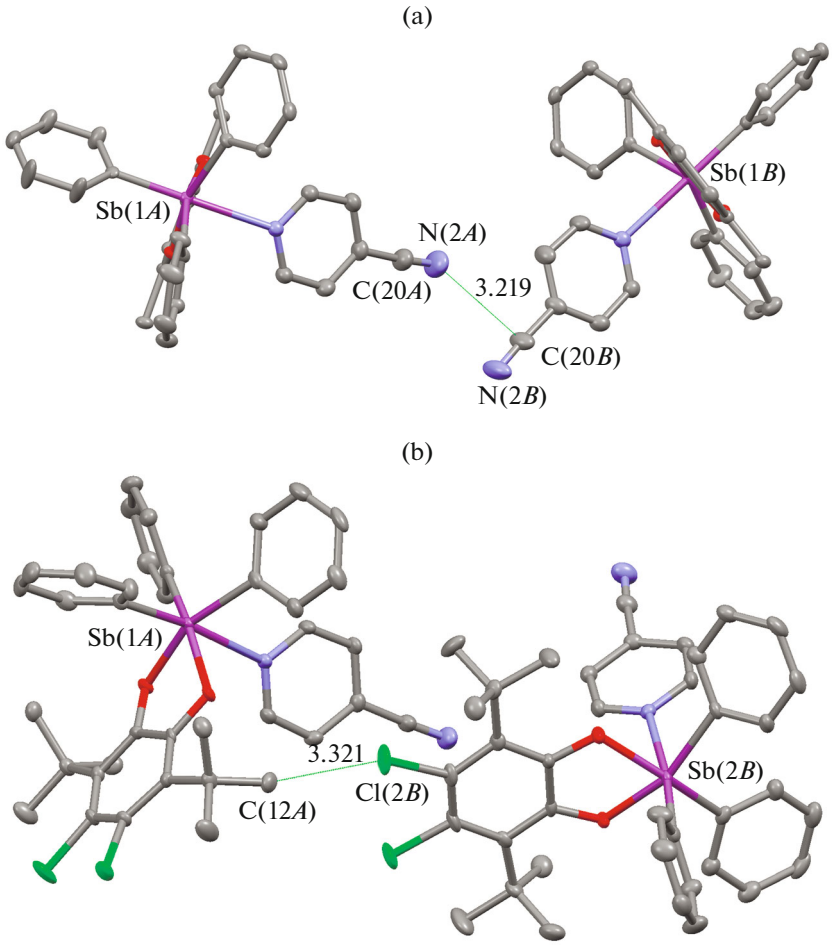

Fig. 6. Intermolecular interactions (Å) in complexes (a) **V** and (b) **VI**. *tert*-Butyl groups and hydrogen atoms are omitted.

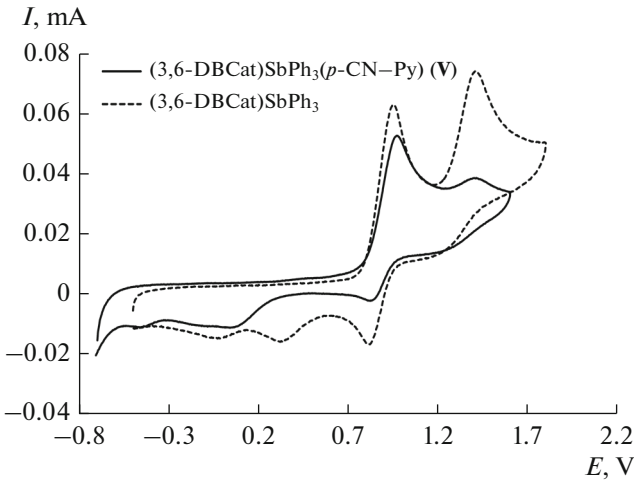

Fig. 7. CV curves for (solid curve) complex **V** (CH_2Cl_2, GC anode, $c = 3 \times 10^{-3}$ mol/L, 0.1 M NBu_4ClO_4, $Ag/AgCl/KCl_{sat}$) at the potential sweep from –0.7 to 1.6 V and (dashed curve) the initial catecholate (3,6-DBCat)$SbPh_3$ at the potential sweep from –0.5 to 1.9 V.

CONFLICT OF INTEREST

The authors declare that they have no conflicts of interest.

REFERENCES

1. Sun, H., *Biological Chemistry of Arsenic, Antimony and Bismuth*, Singapore: Wiley, 2011, p. 400.
2. Tirmenstein, M.A., Plews, P.I., Walker, C.V., et al., *Toxicol. Appl. Pharmacol.*, 1995, vol. 130, no. 1, p. 41.
3. Kato, K.C., Morais-Teixeira, E., Reis, P.G., et al., *Antimicrob. Agents Chemother.*, 2014, vol. 58, no. 1, p. 481.
4. Sharma, P., Perez, D., Cabrera, A., et al., *Acta Pharmacol. Sin.*, 2008, vol. 29, p. 881.
5. Lizarazo-Jaimes, E.H., Reis, P.G., Bezerra, Fi.M., et al., *J. Inorg. Biochem.*, 2014, vol. 132, p. 30.
6. Smolyaninov, I.V., Antonova, N.A., Poddel'sky, A.I., et al., *J. Organomet. Chem.*, 2011, vol. 696, no. 13, p. 2611.

7. Smolyaninov, I.V., Antonova, N.A., Poddel'sky, A.I., et al., *Dokl. Chem.*, 2012, vol. 443, no. 1, p. 72. https://doi.org/10.1134/S0012500812030020
8. Gordon, A. and Ford, R., *The Chemist's Companion: A Handbook of Practical Data, Techniques, and References*, New York: Wiley, 1972.
9. Cherkasov, V.K., Grunova, E.V., Poddel'sky, A.I., et al., *J. Organomet. Chem.*, 2005, vol. 690, p. 1273.
10. Poddel'sky, A.I., Smolyaninov, I.V., Berberova, N.T., et al., *J. Organomet. Chem.*, 2015, vols 789–790, p. 8.
11. Poddel'sky, A.I., Smolyaninov, I.V., Kurskii, Yu.A., et al., *J. Organomet. Chem.*, 2010, vol. 695, p. 1215.
12. Okhlopkova, L.S., Poddel'sky, A.I., Smolyaninov, I.V., et al., *J. Organomet. Chem.*, 2019, vol. 897, p. 32.
13. *SAINT. Data Reduction and Correction Program. Version 8.38A*, Madison: Bruker AXS, 2017.
14. *Data Collection, Reduction and Correction Program, CrysAlis Pro—Software Package*, Agilent Technologies, 2015.
15. Sheldrick, G.M., *Acta Crystallogr. Sect. A: Found. Adv.*, 2015, vol. 71, p. 3.
16. Sheldrick G.M., *SHELXTL. Version 6.14. Structure Determination Software Suite*, Madison: Bruker AXS, 2003.
17. Sheldrick G.M., *SADABS. Version 2016/2. Bruker/Siemens Area Detector Absorption Correction Program*, Madison: Bruker AXS, 2016.
18. *SCALE3 ABSPACK: Empirical Absorption Correction, CrysAlis Pro—Software Package*, Agilent Technologies, 2012.
19. Lide, D.R., *CRC Handbook of Chemistry and Physics*, Boca Raton: CRC Press, 2005.
20. Pierpont, C.G., *Coord. Chem. Rev.*, 2001, vols. 219–221, p. 415.
21. Pierpont, C.G. and Buchanan, R.M., *Coord. Chem. Rev.*, 1981, vol. 38, no. 1, p. 45.
22. Holmes, R.R., Day, R.O., Chandrasekhar, V., et al., *Inorg. Chem.*, 1987, vol. 26, p. 157.
23. Gibbons, M.N., Begley, M.J., Blake, A.J., et al., *J. Chem. Soc., Dalton Trans.*, 1997, p. 2419.
24. Protasenko, N.A., Poddel'sky, A.I., Smolyaninov, I.V., et al., *Russ. Chem. Bull.*, 2014, vol. 63, no. 4, p. 930.
25. Poddel'sky, A.I., Smolyaninov, I.V., Kurskii, A.Yu., et al., *Russ. Chem. Bull.*, 2009, vol. 58, no. 3, p. 532. https://doi.org/10.1007/s11172-009-0052-0
26. Smolyaninov, I.V., Poddel'sky, A.I., Berberova, N.T., et al., *Russ. J. Coord. Chem.*, 2010, vol. 36, p. 644. https://doi.org/10.1134/S1070328410090022
27. Poddel'sky, A.I., Smolyaninov, I.V., Fukin, G.K., et al., *J. Organomet. Chem.*, 2016, vol. 824, p. 1.
28. Poddel'sky, A.I., Druzhkov, N.O., Fukin, G.K., et al., *Polyhedron*, 2017, vol. 124, p. 41.
29. Poddel'sky, A.I., Arsenyev, M.V., Astaf'eva, T.V., et al., *J. Organomet. Chem.*, 2017, vol. 835, p. 17.
30. Arsen'ev, M.V., Okhlopkova, L.S., Poddel'skii, A.I., et al., *Russ. J. Coord. Chem.*, 2018, vol. 44, p. 162. https://doi.org/10.1134/S1070328418020021
31. Poddel'sky, A.I., Smolyaninov, I.V., Fukin, G.K., et al., *J. Organometal. Chem.*, 2018, vol. 867, p. 238.
32. Poddel'sky, A.I., Astaf'eva, T.V., Smolyaninov, I.V., et al., *J. Organomet. Chem.*, 2018, vol. 873, p. 57.
33. Poddel'sky, A.I., Okhlopkova, L.S., Meshcheryakova, I.N., et al., *Russ. J. Coord. Chem.*, 2019, vol. 45, p. 133. https://doi.org/10.1134/S1070328419010093
34. Batsanov, C.C., *Zh. Neorg. Khim.*, 1999, no. 12, p. 3015.

Translated by E. Yablonskaya